JOURNAL OF MATERIALS SCIENCE 31 (1996) 3249–3257

On the elastic properties of rubber toughened Styrenics

C. MAESTRINI*, K. PISONI
Enichem Research Centre, Via Taliercio 14, 46100 Mantova, Italy
H.H. KAUSCH
Laboratoire de Polymères - Departement de Materiaux, Ecole Polytechnique Fédérale de Lausanne, Ecublens, 1015 Lausanne, Switzerland

Rubber toughened Styrenics represent an interesting model system for a blend containing a soft second phase in the form of dispersed spherical particles. The elastic properties of such a system have been widely examined in the past, both from experimental and theoretical viewpoints, however some questions remain unanswered. In this work an attempt is made to rationalize the field via the proposal of pertinent experimentation followed by a short review and the application of a convincing theoretical model. The elastic properties of rubber toughened Styrenics appear to be reproduced by a diluted model for spherical inclusions, in which the lower bound condition has to be used to describe the elastic properties of the second phase particles. Also, the more phenomenological Nielsen equation closely reproduces the experimental data.
These results suggest that the role of stress intensification around the particles in rubber toughened Styrenics has to be reconsidered.

1. Introduction

Rubber toughened Styrenics (RTS), i.e. high impact polystyrene (HIPS) and acrylonitrile-styrene-butadiene (ABS), have great practical relevance, being used in a large variety of everyday applications (packaging, refrigerators, automotive, etc.). Furthermore they represent interesting and relatively simple model systems for the rubber toughening of brittle polymeric matrices. As a result, the interest in their mechanical properties is vast, both from the practical and fundamental points of view.

Concerning the elastic moduli at room temperature, an important experimental study goes back to the early seventies: Cigna [1] demonstrated that the shear moduli of a series of HIPS did not only depend on the rubbery content, but were influenced by a more complex parameter, the *rubbery phase volume fraction*, ϕ, that accounted for the geometrical and structural complexities of the rubbery particles. The work of Cigna represented a crucial advance in the understanding of RTS and has been referenced in many papers and used in daily characterization routines for the last twenty years.

Recently, however, some details in the Cigna work have been criticized by one of us [2, 3]: namely the way of measuring ϕ. Maestrini *et al.* [2, 3] have proposed a stereological method, applied to the analysis of transmission electron microscopy (TEM) pictures, that overcomes the drawbacks inherent in phase separation techniques. This method has been subsequently confirmed by Anzaldi *et al.* [4] by means of physico–chemical considerations and an experimental modification of the routine phase separation measurements.

Following the stereological method described in references [2 and 3] the elastic characteristics of RTS show an observable dependence on the morphology and structure of the second phase which was not discussed in the work of Cigna. This fact is however not completely new and has been reported, for example, for rubber toughened polymethyl metacrylate (PMMA) [5], in which the determination of ϕ does not involve the same difficulties present for HIPS. However, to our knowledge, no convincing rationalization or detailed analysis of these experimental data has been proposed.

Therefore, the aim of this work is:

(a) to present an accurate structural and morphological characterization and the corresponding elastic data for a large set of RTSs (HIPSs and ABSs); and

(b) to discuss them in order to gain a deeper understanding of the role played by the second phase structure and morphology on the mechanical properties.

Dedicated to Dr Giuseppe Cigna in the occasion of his retirement.
*Author to whom correspondence should be addressed.

0022–2461

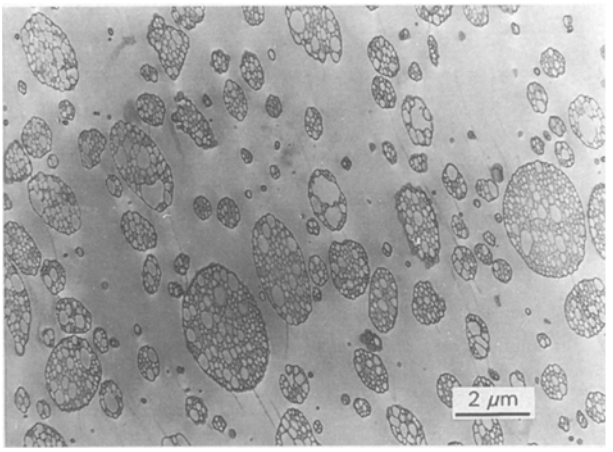

Figure 1 TEM picture of a bulk polymerized HIPS containing composite particles.

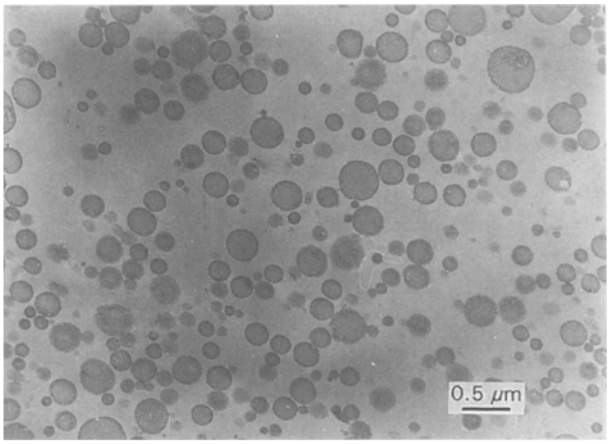

Figure 3 TEM picture of an emulsion polymerized ABS containing bulk particles.

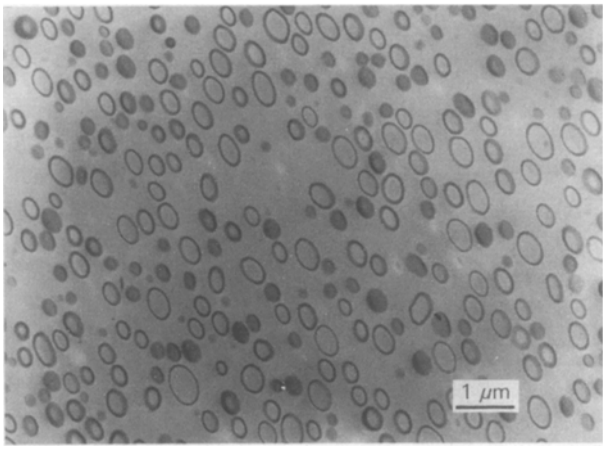

Figure 2 TEM picture of a suspension polymerized HIPS containing core–shell particles.

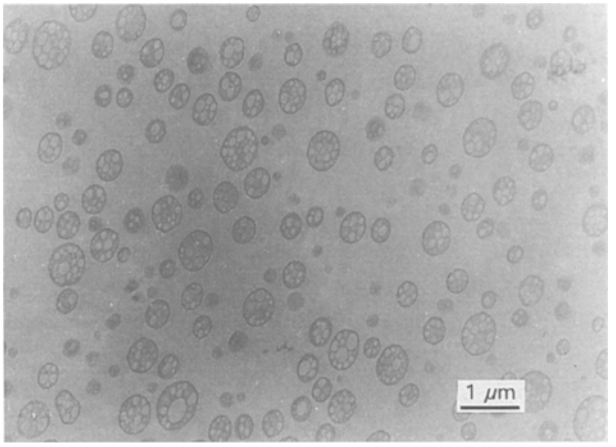

Figure 4 TEM picture of a bulk polymerized ABS containing composite particles.

2. Experimental procedure

2.1. Materials

HIPS is mainly produced by the well documented *bulk polymerization* technique [6–8]. The formation of the rubbery phase ordinarily follows the phase inversion stage and gives rise to a population of well dispersed, more or less spherical particles often having a composite structure similar to that of a *salami* sausage slice. The particles are generally composed of polybutadiene (PB), styrene–butadiene graft and/or block copolymer and of polystyrenic (PS) sub-inclusion: the particle size and number and, also the rubbery phase volume fraction, depend on several process parameters (see Fig. 1 for an example of bulk polymerized HIPS with composite particles).

HIPS can also be produced by the *suspension polymerization* technique [8], modified by the presence of PS–PB copolymer in the initial solution. In this way it is easy to obtain spherical particles with core–shell structures, i.e. composed of a core of PS and an outer shell of PB (see Fig. 2 for an example of suspension polymerized HIPS with core–shell particles).

ABS is traditionally produced by the *emulsion polymerization* technique [6, 7] which can be summarized as follows. (a) The rubbery phase is prepared in the form of latex: (b) PB bulk particles are then dispersed in an aqueous medium; (c) styrene–acrylonitrile is then copolymerized in the presence of the rubber latex in order to obtain a grafted shell covering the particles; the obtained grafted second phase is then dispersed in a matrix of poly(styrene–*r*–acrylonitrile) (SAN) (see Fig. 3 for an example of emulsion polymerized ABS with bulk rubber particles).

Recently the bulk polymerization technique has been adopted for ABS production [9]: in this case the material obtained shows a second phase having a structure very similar to that of the composite HIPS particles polymerized by the same method (see Fig. 4 for an example of bulk polymerized ABS with composite particles).

In the present work we examined sets of materials for each described polymerization technique: Table I contains the data of interest. Much of this data has already been presented in previous publications in which the focus was on properties other than the elastic properties: in these cases Table I indicates the original reference.

TABLE I Materials indicated with the letter *h* are HIPS, with the letter *a* are ABS. The meaning of the symbols is discussed in the text, we remember here that ϕ is the second phase volume fraction of the whole material, while *c* represents the volume fraction of the rigid phase in the particles. (*): The materials are discussed in the reference, but the elastic data are presented for the first time here.

Material	Particle structure	Reference	ϕ	$\langle R^1 \rangle$ μm	ρ	*c*	*E* MPa	μ MPa
*h*1	composite	2	0.069	0.24	0.02	0.76	2849	1163
*h*2	composite	2	0.133	0.24	0.03	0.74	2500	1022
*h*3	composite	2	0.193	0.24	0.05	0.74	2177	857
*h*4	composite	2	0.249	0.24	0.07	0.73	1886	736
*h*5	composite		0.050	0.16	0.02	0.69	3053	1235
*h*6	composite		0.100	0.16	0.03	0.69	2635	1108
*h*7	composite		0.200	0.16	0.06	0.69	2060	854
*h*8	composite		0.050	0.37	0.01	0.79	3051	1227
*h*9	composite		0.100	0.37	0.02	0.79	2648	1086
*h*10	composite		0.200	0.37	0.04	0.79	2162	830
*h*11	composite		0.300	0.37	0.06	0.79	1564	660
*h*12	core–shell	2	0.031	0.11	0.02	0.47	2945	1256
*h*13	core–shell	2	0.054	0.11	0.03	0.47	2763	1127
*h*14	core–shell	2	0.079	0.11	0.04	0.47	2555	1049
*h*15	core–shell	2	0.103	0.11	0.05	0.47	2376	934
*h*16	core–shell	27	0.138	0.08	0.09	0.38	2007	881
*h*17	core–shell	27	0.157	0.09	0.08	0.46	1853	774
*h*18	core–shell	27	0.172	0.09	0.09	0.48		
*h*19	core–shell	27	0.153	0.09	0.09	0.41	2105	819
*h*20	core–shell	27	0.189	0.10	0.09	0.53	1837	728
*h*21	core–shell	27	0.173	0.10	0.09	0.50	2024	791
*h*22	core–shell	27	0.175	0.10	0.10	0.45	2053	777
*h*23	core–shell		0.050	0.10	0.03	0.49	2885	1148
*h*24	core–shell		0.100	0.10	0.05	0.49	2394	984
*a*1	bulk	11 (*)		0.05	0.05	0.00	3443	
*a*2	bulk	11 (*)		0.05	0.10	0.00	2809	
*a*3	bulk	11 (*)		0.05	0.15	0.00	2602	
*a*4	bulk	11 (*)		0.05	0.20	0.00	2311	
*a*5	bulk	11 (*)		0.09	0.05	0.00	3490	
*a*6	bulk	11 (*)		0.09	0.10	0.00	3334	
*a*7	bulk	11 (*)		0.09	0.15	0.00	2898	
*a*8	bulk	11 (*)		0.09	0.20	0.00	2431	
*a*9	composite	11 (*)	0.045	0.13	0.03	0.37	3577	
*a*10	composite	11 (*)	0.091	0.13	0.06	0.37	2860	
*a*11	composite	11 (*)	0.136	0.13	0.09	0.37	2831	
*a*12	composite	11 (*)	0.174	0.13	0.11	0.37	2563	
*a*13	composite	11 (*)	0.064	0.21	0.03	0.56	3440	
*a*14	composite	11 (*)	0.127	0.21	0.06	0.56	3111	
*a*15	composite	11 (*)	0.191	0.21	0.08	0.56	2723	
*a*16	composite	11 (*)	0.244	0.21	0.11	0.56	2423	
*a*17	composite	11 (*)	0.102	0.68	0.03	0.73	3331	
*a*18	composite	11 (*)	0.205	0.68	0.06	0.73	2402	
*a*19	composite	11 (*)	0.307	0.68	0.08	0.73	2153	
*a*20	composite	11 (*)	0.402	0.68	0.11	0.73	1857	
PS							3351	1351
SAN							3705	1400

2.2. Structural and morphological characterization

In order to realize a very precise and quantitatively useful structural characterization, an accurate determination of the particle size distribution and of the rubbery phase volume fraction is necessary. The ordinary method of measuring these two key parameters is, in fact, subject to heavy criticism and gives rise to data that cannot be considered realistic [2, 3]. For this reason, we have adopted the stereological approach described in detail in references [2 and 3]. This consists of analysing transmission electron microscopy (TEM) pictures, obtained by the standard techniques reported in references [10], from material slices having different thickness and then reconstructing the bulk situation. We used the following equations [3]:

$$\langle r^1 \rangle = \frac{\pi \langle R^2 \rangle + 2t \langle R^1 \rangle}{4 \langle R^1 \rangle + 2t} \quad (1)$$

$$\langle r^2 \rangle = \frac{4 \langle R^3 \rangle + 3t \langle R^2 \rangle}{6 \langle R^1 \rangle + 3t} \quad (2)$$

$$\phi_{app} = \frac{4 \langle R^3 \rangle + 3t \langle R^2 \rangle}{4 \langle R^3 \rangle} \phi \quad (3)$$

where the $\langle r^i \rangle$ represents the *i*-th moment of the particle radius distribution in the TEM images, $\langle R^j \rangle$ the *j*-th moment of the real particle distribution in the

bulk, t the observed section thickness, ϕ_{app} the apparent second phase volume fraction in the TEM images and ϕ the real second phase volume fraction. Equations 1–3, which produce an over-determined system when one considers more than one thickness, have been solved using a simple algorithm, which is discussed in reference [11] and consists of the minimization of the maximum component of a normalized linear error function containing all the parameters $\langle R^j \rangle$ and ϕ. The results of such a characterization are displayed in Table 1.

In order to assess the elastic properties obtained with the mathematical models that we will discuss in the following sections it is important to also know the amount of rubber in the material, since from this the amount of rubber in the dispersed phase can be computed. A practical and precise way to do that is by means of titration methods. The PB percentage values, indicated by the greek letter ρ, are displayed in Table I. In a previous work [11] it has been shown that, for ABS produced by emulsion polymerization, the values of ρ can be assumed to well represent the second phase volume fraction, thus, for materials of that class that are discussed in the present work, only one value of ρ is reported.

2.3. Elastic properties

For the HIPSs, both the Young modulus (E) and the shear modulus (μ) were measured on compression moulded specimens using a three-point bending or a simple torsion geometry, respectively. Measurements were performed in the dynamic regime with sinusoidal strain pulses at a frequency of 1 Hz with the maximum strain restricted to the linear viscoelastic zone, i.e. $< 1\%$.

For the ABSs only E was measured, using the same measurement technique.

Two reference samples of PS and SAN have also been investigated, whilst the PB data were obtained from the literature (from references [12 and 13]: $\mu_{PS}/\mu_{PB} = 1000$ and $\nu_{PB} = 0.49982$).

3. Results and discussion

The problem of computing the elastic properties of a particular composite material consists of two steps:

(i) the determination of the effective elastic moduli of the inclusions, considered as a composite themselves; and (ii) the calculation of the global properties of the materials having inclusions with the characteristics calculated in Step (i).

We will start our consideration with this last point.

For this task a great deal of literature is accessible, both on the general theme of particulate composites and on the more specific topic of HIPS and ABS materials [14–20]. An exhaustive review of this data is beyond the scope of this paper and we will simply limit our discussion to areas of direct interest to this work. The simplest equations that can be introduced consider the upper and lower bounds of the problem, i.e.:

$$P_E = cP_i + (1 - c)P_m \tag{4}$$

$$P_E = \frac{P_i P_m}{cP_m + (1 - c)P_i} \tag{5}$$

where P_m, P_i and P_E represent the elastic moduli of the matrix, of the included phase and of the resulting composite material, respectively, and c is the volume fraction of the inclusions. These equations, however, have been largely experimentally disproved. This fact resulted in the generation of a number of semi-phenomenological models. For instance, Boyce *et al.* [21] chose the Chow [22] model in order to compute the effective elastic properties of HIPS with particle structures similar to that of the materials we are investigating. The Chow model, which describes the general case of elliptical inclusions, reduces to the Kerner equations [15] when spherical particles are considered. The Kerner equations have been demonstrated to contain an unjustified assumption, which is to consider that the inclusion is in a homogeneous state of simple shear deformation, and this assumption is invalid [19, 20]. Despite this inconsistency, these models have been demonstrated to be useful in the ordinary experimental practice. We wish then to introduce a phenomenological model that we consider to be more comprehensive and stimulating, which is represented by the Nielsen equation [18]:

$$\frac{P_m}{P_E} = \frac{1 + ABc}{1 - B\Psi c} \tag{6}$$

where the coefficients A, B and Ψ are given by:

$$A = \frac{1}{k - 1} \tag{7}$$

$$B = \frac{P_m/P_i - 1}{P_m/P_i + A} \tag{8}$$

$$\Psi = 1 + \left(\frac{1 - c_{max}}{c_{max}}\right)c \tag{9}$$

The coefficient k appearing in Equation 7 is the Einstein coefficient and has in our case, due to good adhesion between PS and the rubbery particles, a value of 2.5, which corresponds to a dispersion of spheres without slippage; c_{max} represents the maximum packing fraction of the dispersed phase, for which the more probable values for our HIPSs and ABSs are 0.50, characterizing a random loose packing of equal spheres [18].

The same problem can also be treated from a more rigorous point of view. The simplest way is to consider that the dispersed phase is in a diluted state, i.e. the case in which the interactions between the particles can be neglected, no matter what the size of the representative volume element in which the computations are done. It is possible to prove that in the diluted case:

$$k_E = k_m + ((k_i - k_m)c/(1 + (k_i - k_m)/(k_m + \tfrac{4}{3}\mu_m))) \tag{10}$$

$$\frac{\mu_E}{\mu_m} = 1 - \frac{15(1 - \nu_m)(1 - \mu_i/\mu_m)c}{7 - 5\nu_m + 2(4 - 5\nu_m)\mu_i/\mu_m} \tag{11}$$

where k, μ and ν are the bulk modulus, the shear modulus and the Poisson ratio respectively, and the subscripts E, m and i refer to the global material, to the matrix and to the inclusions. The result was apparently first derived by Dewey [14], based on the elastic solution given by Goodier [23].

Furthermore, in order to overcome the restriction of high dilution, we can adopt the so-called *three phase method* (TPM) [19, 20] for the composite spheres model [17], whose derivation is based only on a self-evident energetic hypotheses. The TPM produces the equations:

$$\frac{k_E - k_m}{k_i - k_m} = \frac{c}{1 + [(1-c)(k_i - k_m)/(k_m + \frac{4}{3}\mu_m)]} \quad (12)$$

$$A\left(\frac{\mu_E}{\mu_m}\right)^2 + 2B\left(\frac{\mu_E}{\mu_m}\right) + C = 0 \quad (13)$$

where

$$\begin{aligned} A &= 8\left(\frac{\mu_i}{\mu_m} - 1\right)(4 - 5\nu_m)\eta_1 c^{10/3} \\ &\quad - 2\left[63\left(\frac{\mu_j}{\mu_m} - 1\right)\eta_2 + \eta_1\eta_3\right]c^{7/3} \\ &\quad + 252\left(\frac{\mu_i}{\mu_m} - 1\right)\eta_2 c^{5/3} \\ &\quad - 50\left(\frac{\mu_i}{\mu_m} - 1\right)(7 - 12\nu_m + 8\nu_m^2)\eta_2 c \\ &\quad + 4(7 - 10\nu_m)\eta_2\eta_3 \\ B &= -2\left(\frac{\mu_i}{\mu_m} - 1\right)(1 - 5\nu_m)\eta_1 c^{10/3} \\ &\quad + 2\left[63\left(\frac{\mu_i}{\mu_m} - 1\right)\eta_2 + 2\eta_1\eta_3\right]c^{7/3} \\ &\quad - 252\left(\frac{\mu_i}{\mu_m} - 1\right)\eta_2 c^{5/3} \\ &\quad + 75\left(\frac{\mu_i}{\mu_m} - 1\right)(3 - \nu_m)\eta_2\nu_m c \\ &\quad + 3/2(15\nu_m - 7)\eta_2\eta_3 \\ C &= 4\left(\frac{\mu_i}{\mu_m} - 1\right)(5\nu_m - 7)\eta_1 c^{10/3} \\ &\quad - 2\left[63\left(\frac{\mu_i}{\mu_m} - 1\right)\eta_2 + \eta_1\eta_3\right]c^{7/3} \\ &\quad - 252\left(\frac{\mu_i}{\mu_m} - 1\right)\eta_2 c^{5/3} \\ &\quad + 25\left(\frac{\mu_i}{\mu_m} - 1\right)(\nu_m^2 - 7)\eta_2 c \\ &\quad - (7 - 5\nu_m)\eta_2\eta_3 \end{aligned}$$

with

$$\begin{aligned} \eta_1 &= (49 - 50\nu_i\nu_m)\left(\frac{\mu_i}{\mu_m} - 1\right) + 35\frac{\mu_i}{\mu_m}(\nu_i - 2\nu_m) \\ &\quad + 35(2\nu_i - \nu_m) \\ \eta_2 &= 5\nu_i\left(\frac{\mu_i}{\mu_m} - 8\right) + 7\left(\frac{\mu_i}{\mu_m} + 4\right) \\ \eta_3 &= \frac{\mu_i}{\mu_m}(8 - 10\nu_m) + (7 - 5\nu_m) \end{aligned}$$

The TPM has some limitations since it is derived from a composite sphere model [17], it applies strictly to the case in which the material is formed by a combination of spherical filler particles having different sizes. Nonetheless the validity of the model can still be good, with the limitation that the inclusions volume fraction should be below the maximum volume fraction of the particles in the aggregate form. Experimental data show, in fact, that the composite sphere model gives a very close prediction of the measured effective uniaxial modulus up to a volume fraction of about 50%, also if the size of the included spheres does vary slightly [24]. It should also be pointed out that the composite spheres model is representative of the behaviour of a wide variety of composite systems, not just those with exactly spherical particles. As long as the particles are not greatly different in shape from a spherical configuration, as in our case, the model would be expected to give a reasonable prediction. The flexibility of the model is due to the fact that the effective properties relate to global averages of stress and strain, which themselves are more dependent on the volume fractions of the various phases, rather than to the fine details of the local geometry [20].

Fig. 5 is a plot of the shear modulus, μ, computed according to the different models discussed up to now, vs. the second phase volume fraction, ϕ, for an ideal two phase system: the computational details are reported in the figure caption.

For the HIPS and ABS structure, we are confident that in the determination of the global elastic properties, the volume fraction c should be very well related to the values of ϕ measured in the way described previously. The matrix is obviously composed of PS or SAN, but we still lack knowledge of the effective elastic moduli of the composite particles.

We are now facing the first problem mentioned previously. In this case the composite can be assumed to be formed by a matrix of PB that can contain a dispersion of PS or SAN having different structures. In general we can assume that, for the particles, the volume fraction of the dispersed rigid phase (PS or SAN) can be estimated as:

$$c = \frac{\phi - \rho}{\phi} \quad (14)$$

Furthermore, we are confident that the elastic moduli of the particles are situated between the two limits

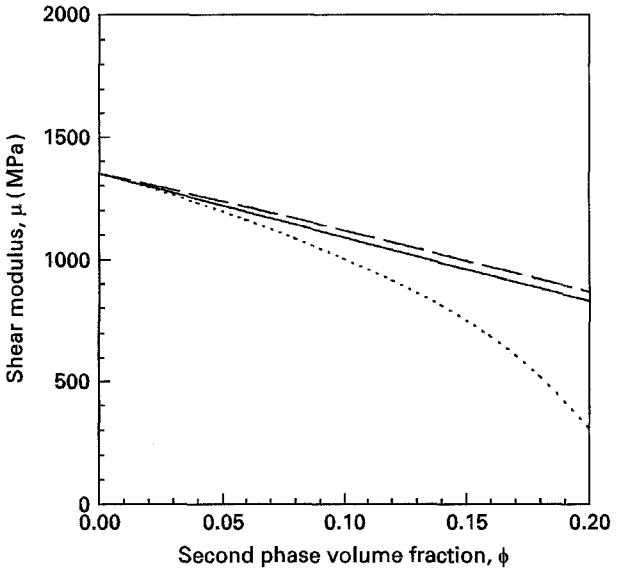

Figure 5 Plot of the shear modulus, μ vs. the second phase volume fraction, ϕ, according to the three theoretical models considered in the text: the Nielsen model (Equations 6–9; dashed line), the diluted model (Equations 10, 11, solid line) and the three phase method (Equations 12, 13, dotted line). The lines are calculated for a system composed by a matrix having $\mu_m = 1351$ MPa, $E_m = 3351$ MPa (corresponding to PS) and spherical inclusions having $\mu_i = 3$ MPa, $E_i = 8$ MPa (corresponding to a computation made by means of the lower bound Equation 5, for core–shell particles with a core of PS, a shell of PB and a core volume fraction of 0.5).

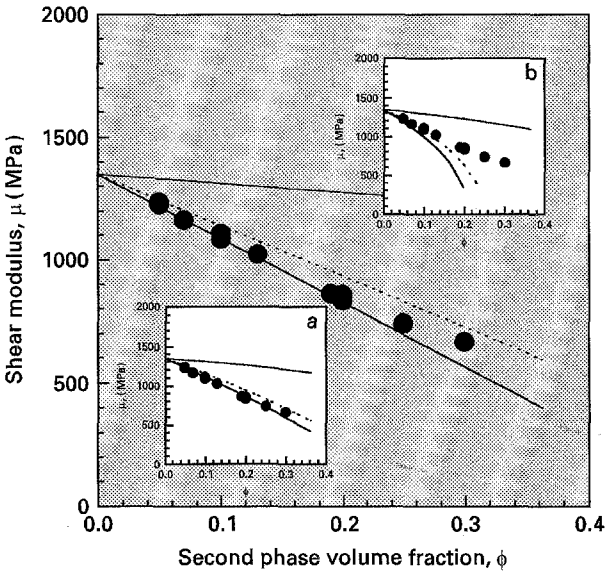

Figure 6 Plot of the shear modulus, μ vs. the second phase volume fraction, ϕ, for materials from *h*1 to *h*11 (HIPS with composite particles). In the main graph are displayed: the experimental data (●); the theoretical curves obtained following the diluted model approach (Equations 10 and 11) in which the elastic characteristics of the dispersed phase are computed by means of the upper and lower bounds (Equations 4 and 5) (——) and the TPM model for the composite spheres (Equations 12 and 13) (.....) using a value of *c* of 0.75. In the minor graph (a) the theoretical curves are obtained from the Nielsen Equation (Equation 6 in the text). The meaning of the symbols and lines is the same as in the main graph. In the minor graph (b) the theoretical curves are obtained from the TPM model (Equations 12 and 13). The meaning of the symbols and lines is the same as in the main graph.

represented by the lower and upper bounds (Equations 4 and 5): it is possible, then, to check the validity of the models above described using these reference values for the rubbery phase properties[1].

Figs 6–12 represent plots of the experimental data and theoretical curves for the considered classes of materials. In the computations we used the known formulae:

$$E = \frac{9k\mu}{3k + \mu} \tag{15}$$

$$\nu = \frac{3k - 2\mu}{2(3k + \mu)} \tag{16}$$

From the examination of the figures it is evident that, with the sole exception of the core–shell HIPS, the elastic behaviour of RTS is well described both by the diluted approach (Equations 10 and 11) and the Nielsen formula (Equation 6), when the rubbery phase properties are computed by means of the lower bound equation and/or the undiluted (TPM) approach (Equations 12 and 13).

Core–shell HIPSs present experimental values lower than those predicted by the diluted approach (Figs 8 and 9): they seem to be quantitatively approximated in a better way by the undiluted (TPM) approach (Equations 12 and 13), however the shape of the experimental data plots does not show the curvature typical of the undiluted approach and more closely resembles the quasi-linearity exhibited by the diluted approach. A possible explanation of this fact can be found in the composition of the core–shell HIPS, which is more complex than ordinary HIPS, containing block-copolymers. It is then possible that the elastic values for PS and PB that we used in the computation may not correspond to the real values of the matrix and the rubber contained in core–shell HIPS. If these values were available and introduced into the computations, it is our opinion that core–shell HIPS would also have been well described by the diluted approach.

The fact that the second phase properties are always well described by the lower bound or by the undiluted (TPM) approach, which are similar, can be explained by the fact that the rubbery particle, and especially in the case of a composite structure, is a dense system in which the interactions between the constitutive parts cannot be neglected.

On the other hand it is not obvious why the RTS systems could be described by a diluted model up to relevant values of ϕ (> 0.3). It is also not straightforward to explain the considerable similarity between the data produced by the diluted approach and the Nielsen formula.

The validity of the diluted model up to large values of ϕ appears, in fact, to be incompatible with classical considerations concerning the stress intensification

[1] In the case of ABS with bulk particles produced by emulsion polymerization the SAN sub-inclusions are virtually absent, so the particle characteristics can be assumed equal to those of pure PB. It is obvious, then, that the above argument does not apply to this class of materials.

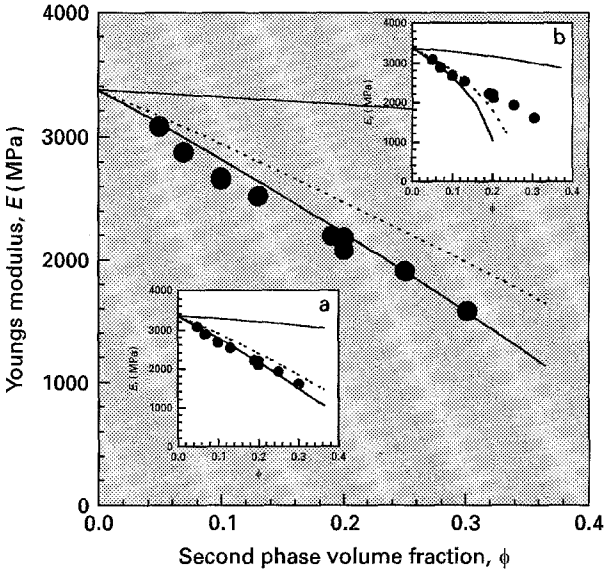

Figure 7 Plot of the Youngs modulus, E vs. the second phase volume fraction, ϕ, for materials from $h1$ to $h11$ (HIPS with composite particles). In the main graph are displayed: the experimental data (●); the theoretical curves obtained following the diluted model approach (Equations 10 and 11) in which the elastic characteristics of the dispersed phase are computed by means of the upper and lower bounds (Equations 4 and 5) (——) and the TPM model for the composite spheres (Equations 12 and 13) (.....) using a value of c of 0.75. In the minor graph (a) the theoretical curves are obtained from the Nielsen Equation (Equation 6 in the text). The meaning of the symbols and lines is the same as in the main graph. In the minor graph (b) the theoretical curves are obtained from the TPM model (Equations 12 and 13). The meaning of the symbols and lines is the same as in the main graph.

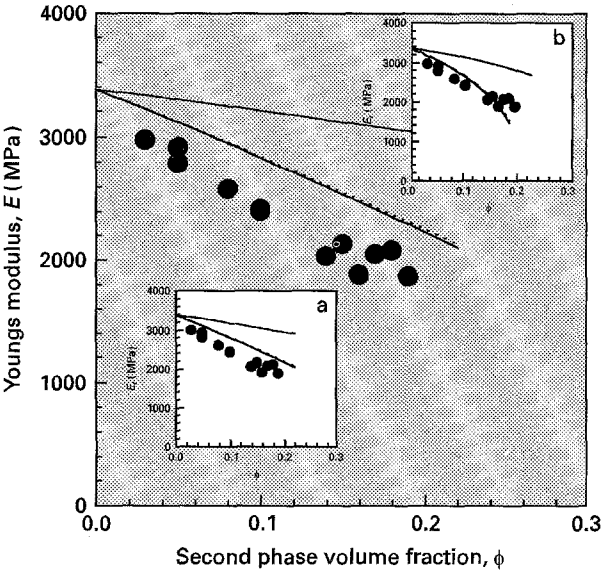

Figure 9 Plot of the Youngs modulus, E vs. the second phase volume fraction, ϕ, for materials from $h12$ to $h24$ (HIPS with core–shell particles). In the main graph are displayed: the experimental data (●); the theoretical curves obtained following the diluted model approach (Equations 10 and 11) in which the elastic characteristics of the dispersed phase are computed by means of the upper and lower bounds (Equations 4 and 5) (——) and the TPM model for the composite spheres (Equations 12 and 13) (.....) using a value of c of 0.75. In the minor graph (a) the theoretical curves are obtained from the Nielsen equation (Equation 6 in the text). The meaning of the symbols and lines is the same as in the main graph. In the minor graph (b) the theoretical curves are obtained from the TPM model (Equations 12 and 13). The meaning of the symbols and lines is the same as in the main graph.

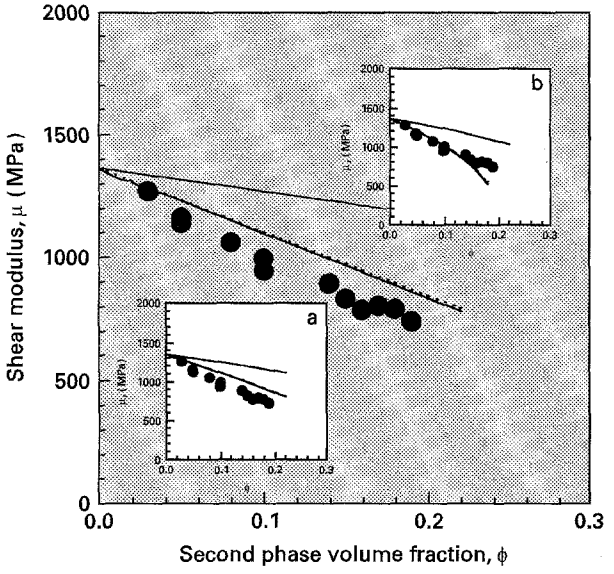

Figure 8 Plot of the shear modulus, μ vs. the second phase volume fraction, ϕ, for materials from $h12$ to $h24$ (HIPS with core–shell particles). In the main graph are displayed: the experimental data (●); the theoretical curves obtained following the diluted model approach (Equations 10 and 11) in which the elastic characteristics of the dispersed phase are computed by means of the upper and lower bounds (Equations 4 and 5) (——) and the TPM model for the composite spheres (Equations 12 and 13) (.....) using a value of c of 0.47. In the minor graph (a) the theoretical curves are obtained from the Nielsen equation (Equation 6 in the text). The meaning of the symbols and lines is the same as in the main graph. In the minor graph (b) the theoretical curves are obtained from the TPM model (Equations 12 and 13). The meaning of the symbols and lines is the same as in the main graph.

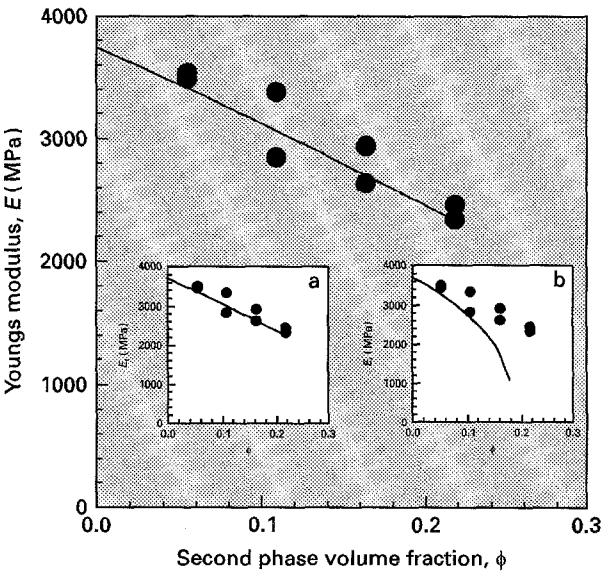

Figure 10 Plot of the Youngs modulus, E vs. the second phase volume fraction, ϕ, for materials from $a1$ to $a8$ (ABS with bulk particles). In the main graph are displayed: the experimental data (●); the theoretical curve obtained following the diluted model approach (Equations 10 and 11) in the text (——). In the minor graph (a) the theoretical curves are obtained from the Nielson equation (Equation 6 in the text). The meaning of the symbols and lines is the same as in the main graph. In the minor graph (b) the theoretical curves are obtained from the TPM model (Equations 12 and 13). The meaning of the symbols and lines is the same as in the main graph.

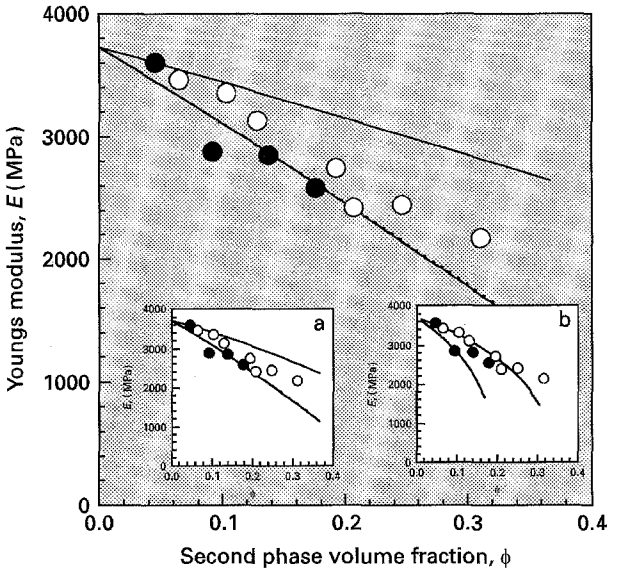

Figure 11 Plot of the Youngs modulus, E vs. the second phase volume fraction, ϕ, for materials from *a*9 to *a*20 (ABS with composite particles). In the main graph are displayed: the experimental data: from *a*9 to *a*12 (●), from *a*13 to *a*20 (○); the theoretical curves obtained following the diluted model approach (Equations 10 and 11) in which the elastic characteristics of the dispersed phase are computed by means of the upper and lower bounds (Equations 4 and 5) (——) and the TPM model for the composite spheres (Equations 12 and 13) (.....) using a value of c of 0.37. In the minor graph (a) the theoretical curves are obtained from the Nielsen equation (Equation 6 in the text). The meaning of the symbols and lines is the same as in the main graph. In the minor graph (b) the theoretical curves are obtained from the TPM model (Equations 12 and 13). The meaning of the symbols and lines is the same as in the main graph.

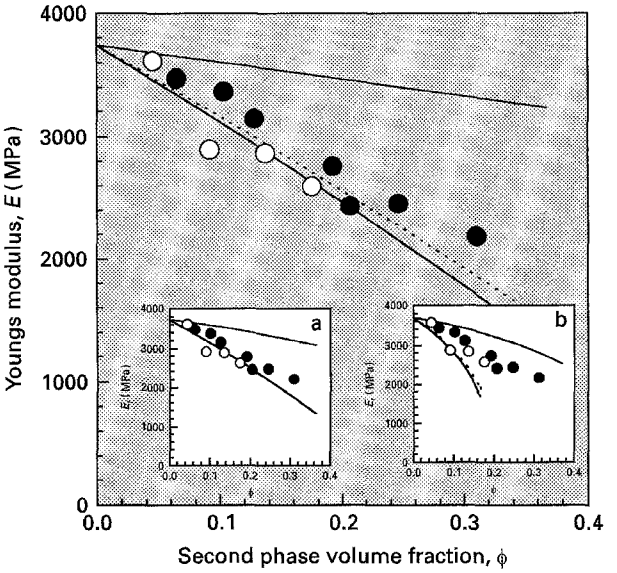

Figure 12 Plot of the Youngs modulus, E vs. the second phase volume fraction, ϕ, for materials from *a*9 to *a*20 (ABS with composite particles). In the main graph are displayed: the experimental data: from *a*9 to *a*12 (○), from *a*13 to *a*20 (●); the theoretical curves obtained following the diluted model approach (Equations 10 and 11) in which the elastic characteristics of the dispersed phase are computed by means of the upper and lower bounds (Equations 4 and 5) (——) and the TPM model for the composite spheres (Equations 12 and 13) (.....) using a value of c of 0.64. In the minor graph (a) the theoretical curves are obtained from the Nielson equation (Equation 6 in the text). The meaning of the symbols and lines is the same as in the main graph. In the minor graph (b) the theoretical curves are obtained from the TPM model (Equations 12 and 13). The meaning of the symbols and lines is the same as in the main graph.

around spherical inclusions. According to Goodier [23], the stress around a rubber particle is amplified to a factor of about 2 and approximately levels out to the nominal applied stress at a distance of about $0.4R$ from the particle–matrix interphase, where R is the particle radius, which means that the intensified stress fields should quickly overlap when the second phase volume fraction increases: the mean particle distance corresponding to a ϕ of 0.3 is, in fact, approximately a value of about $0.4R$. Consequently, if the elastic data obtained by us are to be trusted, one has to conclude that the rubber particles are not as effective as stress intensifiers: the derivation of the diluted approach equations being in open contrast with the stress fields overlapping.

There are other experimental evidences that suggest that the stress intensification and overlap could be questioned in ABS and in core–shell HIPS: namely the fact the yielding stress can be well modelled by means of an extension of the Ishai and Cohen approach, which assumes that no stress intensification and no overlapping takes place [25–27]. It is nontheless evident from the microscopic observation that, at least HIPS composite particles, are very effective as craze nucleating agents, suggesting that the stress conditions around them are surely enhanced [6].

Considering these contradictory indications, our opinion at the present moment is that a stress concentration around the particles is present and is sufficient to nucleate crazes or other kinds of plastic deformation mechanisms, but that it probably falls more quickly than is calculated by means of a pure continuum mechanics approach and, therefore, that the overlapping of the intensified stress fields can be negligible.

This idea can also provide a possible explanation for the considerable similarity observed between the diluted approach and the Nielsen equation. The considerations that produced the Nielsen equation were, in reality, of hydrodynamic nature and involved only the geometric features of the dispersed phase [18]: the Nielsen equation should, then, fail to account for overlapping phenomena and closely reproduce only the non-interacting situation, as is the one outlined in a more rigorous way by the diluted approach.

4. Conclusions

The differences in the elastic behaviour of the studied RTS permit the following interpretation: the elastic moduli of these RTS appear to be well described by the diluted model for spherical inclusions, when the second phase elastic properties are computed, taking into account the internal particle structure, by a lower bound equation or by the three phase model for the composite spheres. The phenomenological Nielsen equation also reproduces the experimental data.

This fact suggests that the way to look at the stress intensification around particles in RTS has possibly to be reconsidered.

Acknowledgements

CM thanks EniChem for the possibility of performing this work in the company's lab in partial fulfillment of the requirement for the degree of Docteur ès Sciences Techniques at EPFL.

References

1. G. CIGNA, *J. Appl. Polym. Sci.* **14** (1970) 1781.
2. C. MAESTRINI, M. MERLOTTI, M. VIGHI and E. MALAGUTI, *Proc. of the European Polymer Federation, 1992*, Baden Baden, 1992.
3. *Idem. J. Mater. Sci.* **27** (1992) 5994.
4. S. ANZALDI, L. BONIFACI, E. MALAGUTI, M. VIGHI and G. P. RAVANETTI, *J. Mater. Sci. Lett.* **33** (94) 1555.
5. P. A. LOVELL, J. MCDONALD, D. E. J. SAUNDERS, M. N. SHERRATT and R. J. YOUNG, in *Toughened Plastics I*, edited by C. K. Riew and A. J. Kinloch, American Chemical Society, Washington, 1993.
6. C. B. BUCKNALL, *Toughened Plastics*, Applied Science Publishers, London, 977.
7. F. RODRIGUEZ, *Principles of Polymer Systems*, McGraw Hill, Singapore, 1983.
8. A. ECTHE, *Rubber Toughened Plastics*, edited by C. K. Riew, American Chemical Society, Washington, 1989.
9. F. BALESTRI, I. BORGHI, S. MATARESSE and C. MAESTRINI, *Proc. Joint. Meet. USSR/Italy Polymer Science*, Leningrad, 1991.
10. K. KATO, *Polym. Eng. Sci.* **7** (1967) 38.
11. G. F. GIACONI, L. CASTELLANI, C. MAESTRINI and T. RICCÒ, *Polymer* (submitted).
12. T. RICCÒ, A. PAVAN and F. DANUSSO, *Polymer* **20** (1979) 367.
13. L. BOHN, *Angew. Makromol. Chem.* **20** (1971) 129.
14. J. M. DEWEY, *J. Appl. Phys.* **18** (1947) 578.
15. E. H. KERNER, *Proc. Phys. Soc.* **69B** (1956) 808.
16. J. D. ESHELBY, *Proc. Roy. Soc.* **A241** (1957) 376.
17. Z. HASHIN, *J. Appl. Mech.* **29** (1962) 143.
18. L. E. NIELSEN, *Predicting the Properties of Mixtures*, Marcel Dekker, New York, 1978.
19. R. M. CHRISTENSEN and K. H. LO, *J. Mech. Phys. Solids* **27** (1979) 4.
20. R. M. CHRISTENSEN, *Mechanics of Composite Materials*, John Wiley & Sons, New York, 1979.
21. M. E. BOYCE, A. S. ARGON and D. M. PARKS, *Polymer* **28** (1987) 1680.
22. T. S. CHOW, *J. Polym. Sci. Polym. Phys. Ed.* **16** (1978) 959.
23. J. N. GOODIER, *J. Appl. Mech.* **55** (1933) 39.
24. T. G. RICHARD, *J. Comp. Mater.* **9** (1975) 108.
25. O. ISHAI and L. COHEN, *J. Compos. Mater.* **2** (1968) 302.
26. T. RICCÒ, M. RINK, S. CAPORUSSO and A. PAVAN, *Proc. 2nd Toughening of Plastics*, London, 1995.
27. C. MAESTRINI, L. MONTI and H. H. KAUSCH, *Polymer*, (in press).

Received 6 March
and accepted 1 December 1995